Electrophoretically deposited graphene oxide and carbon nanotube composite for electrochemical capacitors

2015 Nanotechnology 26 415203

(http://iopscience.iop.org/0957-4484/26/41/415203)

IOP Publishing Nanotechnology
Nanotechnology 26 (2015) 415203 (7pp) doi:10.1088/0957-4484/26/41/415203

Electrophoretically deposited graphene oxide and carbon nanotube composite for electrochemical capacitors

Obafunso A Ajayi[1,7], Daniel H Guitierrez[2], David Peaslee[3], Arthur Cheng[4], Theodore Gao[5], Chee Wei Wong[1,6] and Bin Chen[4]

[1] Department of Mechanical Engineering, Columbia University, New York, NY 10027, USA
[2] Department of Electrical Engineering, Stanford University, CA 94305, USA
[3] Center for Nanoscience and Department of Physics and Astronomy, University of Missouri-St, Louis, St Louis, MO 63121, USA
[4] NASA Ames Research Center, Moffett Field, CA 94035, USA
[5] Northwestern University, Evanston, IL 60208, USA
[6] Department of Mechanical Engineering, University of California, Los Angeles, CA 90094, USA

E-mail: bin-chen1@nasa.gov

Received 13 April 2015, revised 21 July 2015
Accepted for publication 27 August 2015
Published 25 September 2015

Abstract

We report a scalable one-step electrode fabrication approach for synthesizing composite carbon-based supercapacitors with synergistic outcomes. Multi-walled carbon nanotubes (MWCNTs) were successfully integrated into our modified electrophoretic deposition process to directly form composite MWCNT–GO electrochemical capacitor electrodes (where GO is graphene oxide) with superior performance to solely GO electrodes. The measured capacitance improved threefold, reaching a maximum specific capacitance of 231 F g^{-1}. Upon thermal reduction, MWCNT–GO electrode sheet resistance decreased by a factor of 8, significantly greater than the 2× decrease of those without MWCNTs.

Keywords: supercapacitors, carbon-based, electrophoretic deposition

(Some figures may appear in colour only in the online journal)

1. Introduction

Concerns about sustainability and adverse climate effects of fossil fuels have initiated greater exploration into renewable energy technologies. As greater advances are being made in technologies such as solar and wind power generation, and electric/hybrid vehicles, a concomitant development of low-cost and high performance energy storage systems is required. Electrochemical capacitors, also known as supercapacitors or ultracapacitors, are at the forefront of promising energy storage systems due to their high specific capacitance, high specific power, energy density and long life cycles as well as low material cost and toxicity [1–6]. Although some have been found to perform with power densities several thousands of times higher than those of lithium ion batteries [7], they are limited by their comparatively low energy densities of approximately 2.6 to 15 times smaller than that of batteries [8]. Electrochemical capacitors that could achieve both high power and energy density are imperative for a wide range of applications from renewable energy to portable electronics.

Energy storage in electrochemical capacitors occurs through two types of capacitive mechanisms: electric double layer capacitance or fast and reversible Faradic redox reactions, known as pseudocapacitance. In electrical double layer (EDL) capacitance, charge is stored electrostatically at the electrode–electrolyte interface through reversible ion adsorption–desorption. With large surface area interfaces, the electrostatic charge mechanism facilitates rapid charge/discharge rate capability, higher power density and high reversibility that lends to a potentially limitless cycle life [1–3].

[7] This research was performed while Ajayi was at NASA Ames Research Center.

Due to the surface-specific nature of the charging mechanism, high surface-area electrode materials are crucial to achieve a high EDL capacitance. Reduced graphene oxide (rGO) has emerged as an attractive EDL electrochemical capacitor material due to the superior mechanical and electronic properties of graphene, including its high specific surface area ($2630\,m^2\,g^{-1}$) [9], high thermal [10] and electrical [11] in-plane conductivity. Although graphene promises a high theoretical EDL capacitance ($550\,F\,g^{-1}$) its utilization in commercial applications depends on research breakthroughs to overcome its typically high-cost of fabrication and various performance challenges [12].

Although graphene synthesis methods such as mechanical exfoliation and chemical vapor deposition have been shown to produce high quality graphene, they suffer from low yield and high cost, respectively. Chemical reduction of GO has emerged as an alternate method for inexpensive and scalable mass production of graphene-like films. In this process graphite is oxidized via a modified Hummers method where the oxygen-based surface functionalization weakens inter-layer bonds, leading to monolayer (or few layer) exfoliation of graphite producing GO. It is then reduced to remove functional groups, restore sp^2 bonding, and has been shown to exhibit properties approaching pristine graphene [13–15].

Several studies have investigated the performance of rGO electrochemical capacitor electrodes demonstrating specific capacitances of $117\,F\,g^{-1}$ in aqueous H_2SO_4, [16] $135\,F\,g^{-1}$ in aqueous KOH electrolyte, and $99\,F\,g^{-1}$ in organic electrolyte [17]. Later, $205\,F\,g^{-1}$ was achieved in KOH aqueous solution [6]. Capacitances as high as $243.7\,F\,g^{-1}$ [18] and $265\,F\,g^{-1}$ [12] have been reached for in-plane parallel graphene sheets and laser-induced graphite oxide reduction, respectively. Interlayer van der Waals interactions are thought to reduce the accessible surface area through restacking of graphene sheets, which reduces the double layer area resulting in a less than ideal performance [19, 20]. To enhance the surface area accessibility of chemically modified graphene sheets, several approaches have been proposed to prevent aggregation of sheets including multi walled carbon nanotubes (MWCNT) as one-dimensional spacers between the graphene sheets [21–25]. They are further believed to be a suitable complementary material in rGO electrochemical capacitors due to their high electrical conductivity ($10^4\,S\,m^{-1}$) and high surface area. Hybrid rGO–MWCNT composite electrochemical capacitors have achieved a specific capacitance as high as $326.5\,F\,g^{-1}$ [23].

Several fabrication methods for rGO–MWCNT electrochemical capacitor electrodes have been employed including layer-by-layer deposition [21, 26], other solution-based deposition methods (i.e. dip coating, spray coating, spin-casting) or membrane vacuum filtration [27–29]; however, they can be time-consuming or lack the capability for controlled deposition or scalability. Electrophoretic deposition (EPD) is an alternative method that may be used to obtain binder-free carbon nanotube-graphene composite electrochemical capacitor electrodes. EPD provides an economical means of achieving controlled uniform deposition at high rates. This method has been shown to provide additional reduction of GO during deposition [30, 31] and to reduce the equivalent series resistance in carbon nanotubes electrodes [32, 33]. In this study we capitalize on these benefits and investigate the resulting capacitive properties of hybrid RGO–MWCNT electrochemical capacitors fabricated by EPD.

2. Methods

2.1. Material synthesis

All chemicals and substances used were purchased from Sigma-Aldrich. Graphene oxide (GO) was synthesized from synthetic graphite (<20 μm flakes) via a previously reported modified Hummers' method with additional $KMnO_4$ [34]. MWCNT were prepared by refluxing 1 g multi-walled MWCNTs, 1.875 mL nitric acid and 5.625 mL sulfuric acid for 30 min at 130 °C [35]. The MWCNTs were separated from the solution by centrifuging and decanting the top solution. They were further washed repeatedly with DI water, dried and weighed before being transferred to dimethylformamide, which has been found to be the best solvent for high concentration solutions [33].

2.2. EPD and reduction

Mixed-solvent solutions containing GO and MWCNTs were prepared in two steps. The first step produced a final GO colloidal solution with concentration of $0.75\,mg\,mL^{-1}$ [36]. The solution containing GO and MWCNTs was prepared by adding varying wt% MWCNTs to the GO–water colloidal solution. A modified EPD (mEPD) was performed in accordance to a previous study [36] with a 50 V bias at room temperature. Both electrodes were made of 316 stainless steel plates. The mEPD method utilized [36] employed horizontal substrate alignment (with the deposition substrate on the bottom), which minimized the affects of turbulence from gas bubble formation. Substrates were mechanically pulled out at $1.4\,mm\,min^{-1}$ while still under the applied voltage. The average thickness of deposited material could be varied as it is directly proportional to the length of time or voltage during mEPD.

Thermal reduction of the GO and GO–MWCNT electrodes was performed with a Lindberg/Blue MiniMite tube furnace at 300 °C for 1 h in air with a slow ramp-up rate of $3\,°C\,min^{-1}$.

2.3. Characterization

Electrochemical measurements were performed with a CHI 650B Electrochemical Workstation (CH Instruments) in a three probe set up. The standard AG/AgCl electrode and a platinum mesh acted as reference and counter electrodes, respectively. Our liquid cells were manufactured in-house with a 5 mm diameter hole in the base, exposing our electrodes to 3 M KOH. The electrode morphology was imaged using scanning electron microscopy (SEM) (Hitachi S-4800). A sample tilt feature was utilized within the SEM stage to perform depth measurements. Further characterization was

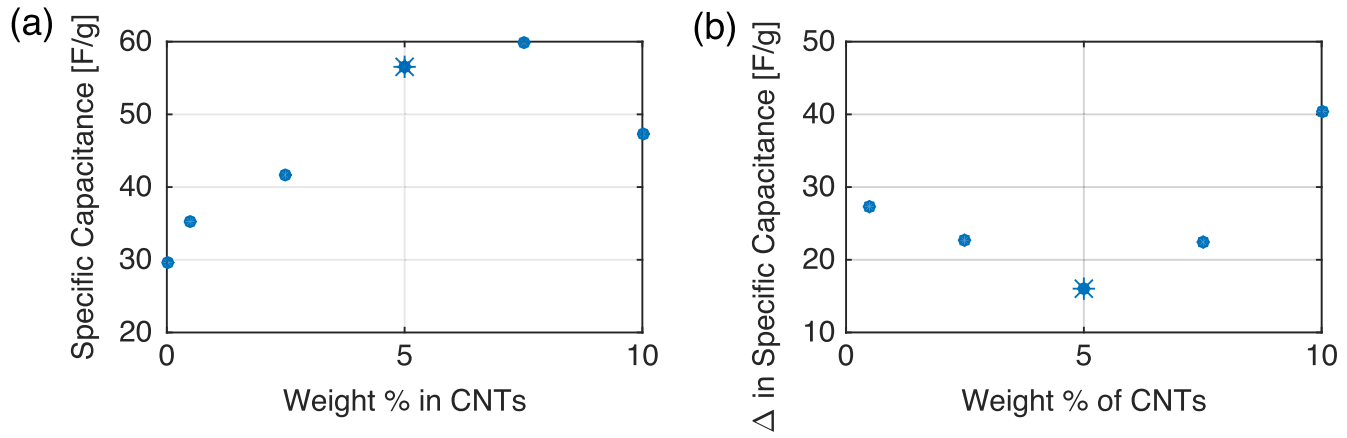

Figure 1. (a) Chart of specific capacitance versus weight % of MWCNT and (b) a chart of the decrease in specific capacitance after 1000 cycles versus weight % of MWCNT. These results show us that around 5% MWCNT by weight is superior in both performance and lifetime.

performed with an inVia Raman microscope (Renishaw) using a 514 nm laser. Fourier Transform Infrared spectroscopy was performed using a Nicolet *Magna-IR Spectrometer* 550. Sheet resistance of the deposited films was evaluated using the Van der Pauw method with a four-point probe. This configuration, which separates the current and voltage probes, provides a powerful tool for selective measurement of the sheet resistance without interference of the high contact resistance in nanoscale devices [37]. Control Van der Pauw four point-probe measurements were taken of the stainless steel substrate to ensure accurate measurements of the composite electrodes. Voltage and current were measured by a Keithley 6514 and Keithley 6220 respectively, controlled by a Labview program. Probes were carefully inserted on the thin-film and monitored, as the resistivity of the underlying stainless steel was orders of magnitude lower than the thin film. Each electrode's active material was weighed with a Mettler AE 240 mass balance.

3. Results and discussions

Different wt% of MWCNT in EPD solutions gave varying characteristics. Experimentation revealed that 5 wt% produced the best combination of both specific capacitance and cycling stability over many hundreds of cycles, as shown in figure 1. With increased MWCNT concentration, a tradeoff between available surface area for conductivity and structural wrinkling of the films due to crowding occurs. An optimal state is reached at 5 wt%. At higher wt%, non-uniform films form, which add mass in the form of inactive material. Superior films were approximately 50–60 μm thick, which corresponded to 3 min of EPD at 50 V.

Adding MWCNT increased the density of charge transport sites, thus mitigating the interlayer resistances in rGO. The average sheet resistance measured on electrodes using the four-point probe is reported in table 1. The sheet resistance of electrodes on stainless steel, GO or composite GO–MWCNT, was measured before and after thermal reduction. Upon reduction the sheet resistance reduced in both GO and GO–MWCNT electrodes. However, the sheet resistance in the GO–MWCNT electrodes was reduced 8 fold after thermal reduction, compared to a 2 fold reduction in the GO electrodes. We attribute this 4× increased conductivity in reduced GO–MWCNT to the CNTs [38].

Table 1. Sheet resistance (R_s) (kΩ sq^{-1}).

Sample	As deposited	Reduced
GO	18.7	8.5
GO–MWCNT	18.6	2.3

The SEM images in figure 2 depict an electrode morphology with a high surface area and improved conduction pathway via a highly connected network, which aides the conductivity of the rGO–MWCNT composites. With SEM we measured the average thickness of our deposition to be 273 μm, before reduction. The reduction process decreased the thickness to 58 μm due to the vaporized solvent and annealing. As seen in figure 2(a), the interconnected network of carbon nanotubes bridge rGO platelets. The MWCNT network provides an electron conduction pathway throughout the composite. Figure 2(a) also indicates that the high porosity in the MWCNT network allowed for electrolyte diffusion. Figure 2(b) inset shows rGO alone. Figure 2(b) shows that the carbon nanotubes also serve to increase the accessible surface area of rGO, and appear to inhibit planar re-stacking between rGO sheets, thus overcoming the van der Waals forces between rGO platelets. This is a significant observation because the MWCNT in the composite can be expected to increase the overall charge storage, leading improved specific capacitance and energy density.

Figures 3 and 4 report the Raman and FTIR spectra, respectively, for the rGO, MWCNT, and rGO–MWCNT electrodes. Raman measurements, as shown in figure 3, provide insight into the morphology of the resulting electrodeposited electrodes. The *G* peak, arising from in-plane C–C bond stretches, is a powerful probe into strain effects, occurs at 1598 nm and 1590 nm for the rGO and MWCNT electrodes respectively. The *D* peak, a double resonance mode that

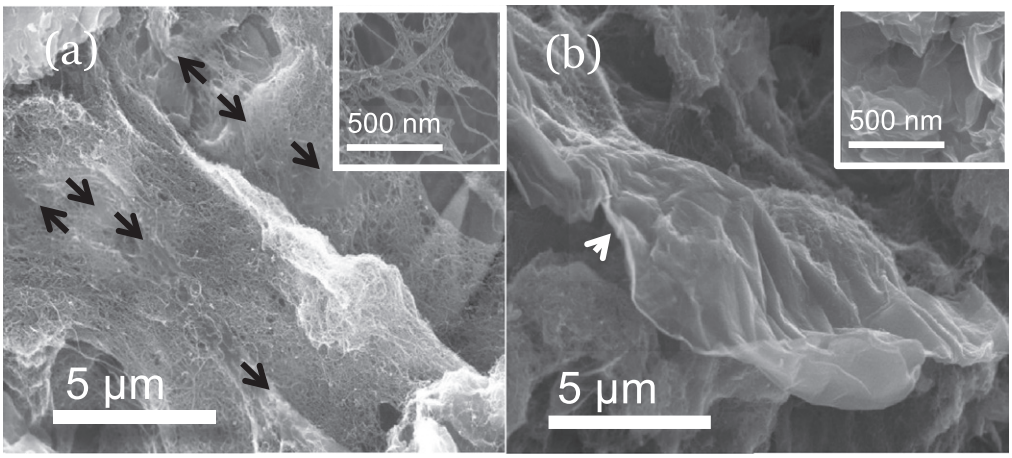

Figure 2. (a) Networked MWCNT connecting rGO platelets. Arrows indicate continuity of rGO–MWCNT–rGO. (Inset) MWCNT network with regions of sizable gaps (hundreds of nm) to allow electrolyte ions through. (b) MWCNT reducing aggregation of rGO sheets. Here the gaps between rGO sheets and MWCNT (as shown by the white arrow) provide additional entrance points for electrolytes, increasing the electrolyte-accessible surface area of rGO. (Inset) rGO alone displaying propensity to aggregate due to van der Waals interactions.

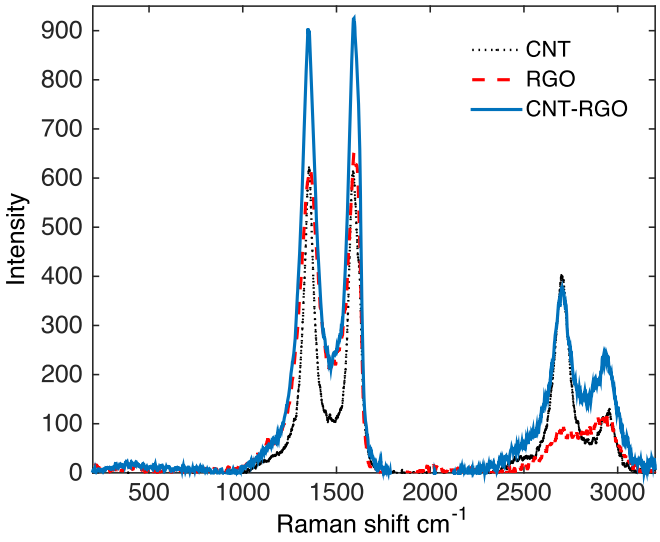

Figure 3. Raman spectra of rGO, MWCNTs and rGO with MWCNTs. The peak ratios of D (1360 cm^{-1}) to G (1560 cm^{-1}) were unaltered during the mEPD process ensuring intactness of the conductive carbon materials.

provides a measure of structural disorder and defects, occurs at ~1353 nm. The $D + G$ peak centered around 2918 and 2938 nm for rGO and MWCNT respectively, also provides a measure into disorder and defects. The G' mode (known also as the 2D) is also a double resonance mode exhibited in sp^2 carbon materials and occurs at 2580–2800 cm^{-1}. As seen in figure 3 MWCNT demonstrates a sharp 2D peak, centered 2701 cm^{-1}, while the rGO 2D peak is broadened and centered at 2688 cm^{-1}. Fourier transform-infrared spectroscopy (FT-IR) further illustrates the efficacy of the reduction of GO (figure 4(a)). Several features are readily discerned from the GO spectra: C–O (epoxy) at ~1000 cm^{-1}, –OH (phenol) at ~1220 cm^{-1}, C=O (carboxyl) ~1700 cm^{-1}. These features are reduced or absent from the rGO spectra (figure 4(a)). The C=C feature present in GO at 1600 cm^{-1} persists in rGO, shifted to 1550 cm^{-1}.

Hybrid rGO–MWCNT Raman spectroscopy reflects the composite nature of the electrodes. Figure 3 shows a well-defined rGO–MWCNT hybrid. Table 2 shows the average values of key Raman spectral features for our rGO, MWCNT and rGO–MWCNT composites. The D to G intensity ratio (I_D/I_G) is taken as a measure of disorder. The D and G peaks, are visually similar in the Raman spectra of rGO and MWCNT. We use the distinctive 2D and $D + G$ features of rGO and MWCNT as a probe for the resulting rGO–MWCNT electrode morphology. The 2D to $D + G$ ratio is higher in MWCNT compared to rGO due to its sharp 2D peak. Also the rGO 2D peak has a broader full-width-half-maximum (FWHM). This broadening has been attributed in part to oxygen groups that are not fully reduced, as the FWHM has been observed to narrow with increasing thermal reduction time [39]. We include the FWHM of the 2D peak in table 2 as an additional direct characterization of the morphology of the electrodes; As noted, rGO can be distinguished from MWCNT by its broader 2D peak. The intermediate rGO–MWCNT composite FWHM captures the presence of both CNTs and rGO. While visual inspection of the rGO–MWCNT SEM images would suggest a predominance of MWCNTs in the resulting composites, Raman spectroscopy reveals that the resulting morphology well incorporates both rGO and MWCNT, as seen in table 2. The hybrid values fall within those of rGO and MWCNT separately. FTIR also demonstrates the composite nature of the rGO–CNT electrodes as seen in figure 4(b). The characteristic asymmetric CH_2 group peaks at 2840 and 2900 cm^{-1} in CNT persist in the rGO–CNT group (shifted up 10 cm^{-1} and 20 cm^{-1} respectively). Additionally the C=C peak is easily discernible at 1560 cm^{-1} in the rGO–CNT electrodes, as it is in rGO.

Cyclic voltammetry at variable scan rates revealed a significant capacitive improvement for the rGO–MWCNT electrode (see figure 5). As illustrated, the rGO–CNT electrodes have a larger integrated CV area, indicative of higher

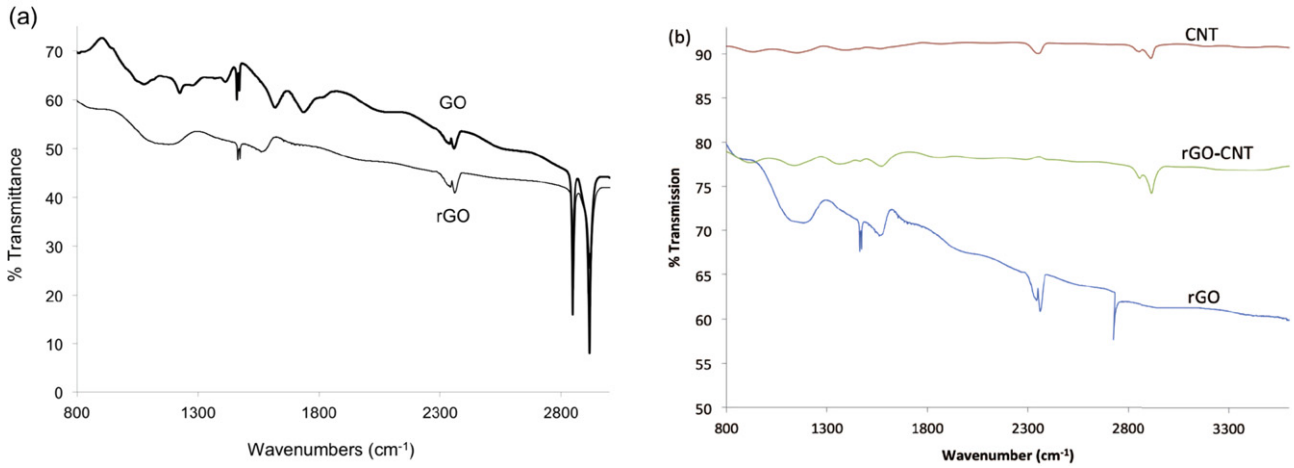

Figure 4. Comparison of the FTIR response between (a) GO and rGO and between (b) rGO, MWCNT alone and rGO with MWCNT.

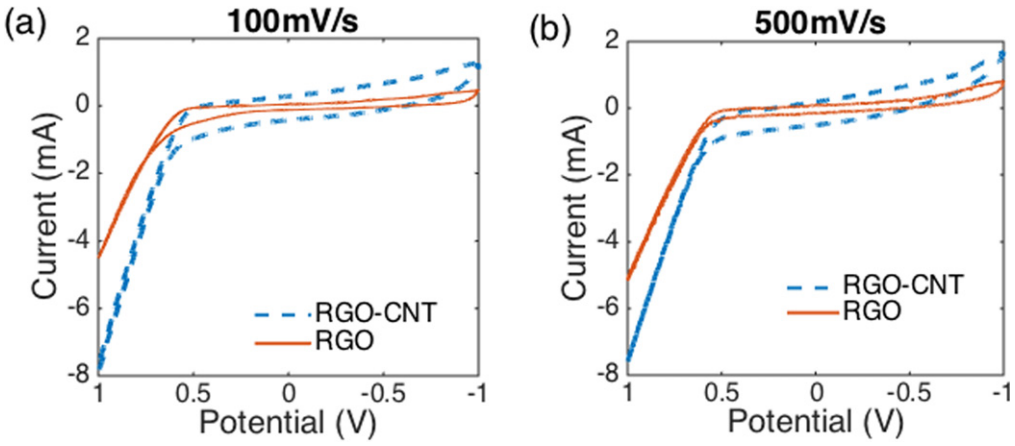

Figure 5. Capacitive response of rGO and rGO–MWCNT electrodes using cyclic voltammetry at (a) 100 mV s^{-1} and (b) 500 mV s^{-1}.

Table 2. Raman spectral features.

	I_D/I_G ratio	I_{2D}/I_{D+G} ratio	$FHWM_{2D}$
rGO	0.93 ± 0.03	0.82 ± 0.09	157.49 ± 4.6
MWCNT	1.02 ± 0.03	3.59 ± 0.50	103.38 ± 17.81
rGO–MWCNT	1.01 ± 0.4	2.03 ± 1.04	133.31 ± 39.03

capacitance. Additionally we observe that both RGO and CNT/rGO curves lack distinctive redox peaks, which typically signify a strong presence of pseudocapacitance. The linear curve shapes are more closely attributed to EDL capacitance, as is typical in carbon-based supercapacitors. However the curve shapes are not rectangular, as expected in an ideal capacitor, but oblique. The oblique angles in the electrode curves are indicative of resistance, potentially contact resistance. We also note the steeper angles between the 100 and 500 mV s^{-1} scan rate also suggesting increased contact resistance with increased scan rate

$$C' = I/(\Delta V/\Delta t), \tag{1}$$

$$C = C'/\text{area or } C'/\text{mass}, \tag{2}$$

$$C_{sp} = 1/2\left(C^{high} - C^{low}\right). \tag{3}$$

Specific capacitance was determined from equations (1)–(3). Here $\Delta V/\Delta t$ is the voltage scan rate and I is the measured current. The deposited mass of the rGO and rGO–MWCNT was found to be 15.7 μg and 18.1 μg, respectively. We calculate the average specific capacitance for the electrodes within the range of stability of −6 to 6 V. The instability is attributed to KOH interacting with the rGO within the composite. At a scan rate of 100 mV s^{-1} the average specific capacitance for the rGO–CNT electrode is 180 F g^{-1} with a maximum value of 223 F g^{-1}.; the rGO electrode has an average specific capacitance of 65 F g^{-1} with a maximum value of 132 F g^{-1} as shown in figure 6(a). Doing a point-by-point comparison the rGO–CNT's supercapacitance is 3.1 times higher than that of rGO at 100 mV s^{-1}. At a scan rate of 500 mV s^{-1} the average specific capacitance for the rGO–CNT electrode is 221 F g^{-1} with a maximum value of 231 F g^{-1}.; the rGO electrode has an average specific

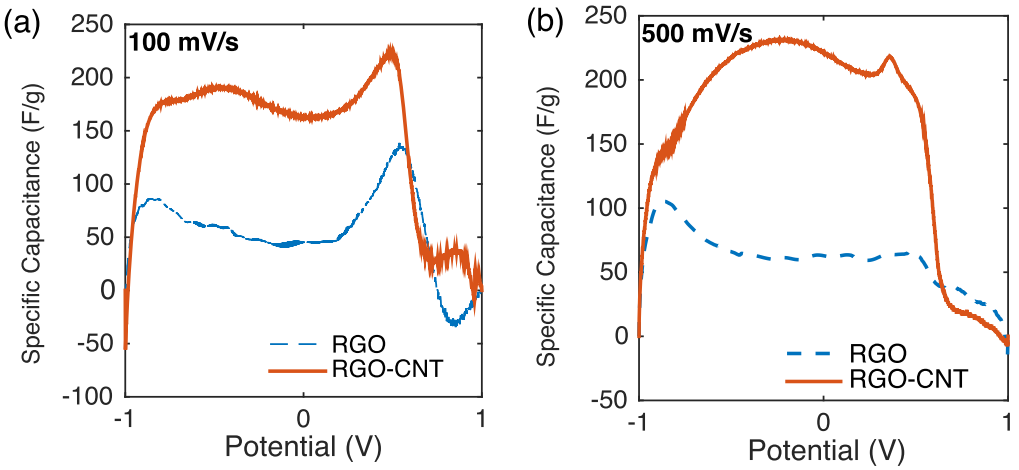

Figure 6. Specific capacitance of rGO and rGO–MWCNT electrodes calculated from equations (1) and (2). We recorded a significant increase in specific capacitance with our rGO–MWCNT electrode. At a scan rate of 100 mV s^{-1} (a) the resulting specific capacitance was on average 3 times larger for the rGO–MWCNT electrode. At a scan rate of 500 mV s^{-1} the resulting capacitance was on average 3.4 times larger for the rGO–MWCNT electrode.

capacitance of 62 F g^{-1} with a maximum value of 91 F g^{-1} as shown in figure 6(b). Doing a point-by-point comparison the rGO–CNT's supercapacitance is 3.4 times higher than that of rGO at 100 mV s^{-1}. The energy density of the rGO–MWCNT electrode was 5.7 kWh kg^{-1}.

4. Conclusion

The composites of MWCNT and rGO were successfully deposited with GO using mEPD and thermal reduction. We have obtained an optimal concentration, 5% by weight, MWCNT to GO that increases the energy density and retains stability after 1000 cycles in our supercapacitor electrodes. The resulting morphology integrates MWCNTs to increase charge injection and to form a conductive pathway to reduce the interlayer resistances. The addition of the MWCNT reduced the sheet resistance by about a quarter and tripled the measured capacitance of the electrochemical capacitor electrodes. The scalability of our mEPD process, its ability to tune deposition thickness and our results thus far will allow us to next demonstrate how our cells, when scaled, has the potential to outperform the industry standard supercapacitors.

Acknowledgments

Special thanks must be given for the support of NASA Senior Scientist, Dr Meyya Meyyapan and Dr Jessica Koehne for their ongoing support of the Advanced Space Science and Technology group. Other contributors to this paper and the ASST group include, Drs Zuki Tanaka, Alisson Engstrom, Cristina Javier. Additional thanks is given to Dr Young Duck Kim and Ghidewon Arefe for fruitful discussions on the electrical measurements. O A A also acknowledges an Engineering Innovation Fellowship through Graduate Research Fellowship Program of the National Science Foundation.

References

[1] Conway B E 1999 *Electrochemical Supercapacitors: Scientific Fundamentals and Technological Applications* (New York: Kluwer)
[2] Kotz R and Carlen M 2000 *Electrochim. Acta* **45** 2483
[3] Chae J H, Ng K C and Chen G Z 2010 *Proc. Inst. Mech. Eng. A* **224** 479
[4] Deng W, Ji X, Chen Q and Banks C E 2011 *RSC Adv.* **1** 1171
[5] Zhao X, Sánchez B M, Dobson P J and Grant P S 2011 *Nanoscale* **3** 839
[6] Wang Y, Shi Z, Huang Y, Ma Y, Wang C, Chen M and Chen Y 2009 *J. Phys. Chem.* C **113** 13103
[7] Pandolfo A G and Hollenkamp A F 2006 *J. Power Sources* **157** 11
[8] Obreja V V N 2008 *Physica* E **40** 2596
[9] Peigney A, Laurent C, Flahaut E, Bacsa R R and Rousset A 2001 *Carbon* **39** 507
[10] Balandin A A, Ghosh S, Bao W, Calizo I, Teweldebrhan D, Miao F and Lau C N 2008 *Nano Lett.* **8** 902
[11] Fang T, Konar A, Xing H and Jena D 2007 *Appl. Phys. Lett.* **91** 092109
[12] El-Kady M F, Strong V, Dubin S and Kaner R B 2012 *Science* **335** 1326
[13] Dreyer D R, Park S, Bielawski C W and Ruoff R S 2009 *Chem. Soc. Rev.* **39** 228
[14] Pei S and Cheng H-M 2012 *Carbon* **50** 3210
[15] Zhu Y, Murali S, Cai W, Li X, Suk J W, Potts J R and Ruoff R S 2010 *Adv. Mater.* **22** 3906
[16] Vivekchand S R, Rout C S, Subrahmanyam K S, Govindaraj A and Rao C N R 2008 *J. Chem. Sci.* **120** 9
[17] Stoller M D, Park S, Zhu Y, An J and Ruoff R S 2008 *Nano Lett.* **8** 3498
[18] Yoo J J *et al* 2011 *Nano Lett.* **11** 1423
[19] Si Y and Samulski E T 2008 *Nano Lett.* **8** 1679
[20] Li D, Müller M B, Gilje S, Kaner R B and Wallace G G 2008 *Nat. Nanotechnology* **3** 101
[21] Yu D and Dai L 2010 *J. Phys. Chem. Lett.* **1** 467

[22] Fan Z, Yan J, Zhi L, Zhang Q, Wei T, Feng J, Zhang M, Qian W and Wei F 2010 *Adv. Mater.* **22** 3723
[23] Yang S-Y, Chang K-H, Tien H-W, Lee Y-F, Li S-M, Wang Y-S, Wang J-Y, Ma C-C M and Hu C-C 2011 *J. Mater. Chem.* **21** 2374
[24] Jha N, Ramesh P, Bekyarova E, Itkis M E and Haddon R C 2012 *Adv. Energy Mater.* **2** 438
[25] Cheng Q, Tang J, Ma J, Zhang H, Shinya N and Qin L-C 2011 *Phys. Chem. Chem. Phys.* **13** 17615
[26] Byon H R, Lee S W, Chen S, Hammond P T and Shao-Horn Y 2011 *Carbon* **49** 457
[27] Lu X, Dou H, Gao B, Yuan C, Yang S, Hao L, Shen L and Zhang X 2011 *Electrochim. Acta* **56** 5115
[28] Huang Z-D, Zhang B, Liang R, Zheng Q-B, Oh S W, Lin X-Y, Yousefi N and Kim J-K 2012 *Carbon* **50** 4239
[29] Yu D, Goh K, Wang H, Wei L, Jiang W, Zhang Q, Dai L and Chen Y 2014 *Nat. Nanotechnology* **9** 555–62
[30] Chen Y, Zhang X, Yu P and Ma Y 2010 *J. Power Sources* **195** 3031
[31] Lee V, Whittaker L, Jaye C, Baroudi K M and Fischer D A 2009 *Chem. Mater.* **21** 3905
[32] Du C and Pan N 2006 *Nanotechnology* **17** 5314
[33] Boccaccini A R, Cho J, Roether J A, Thomas B J C, Jane Minay E and Shaffer M S P 2006 *Carbon* **44** 3149
[34] Marcano D C, Kosynkin D V, Berlin J M, Sinitskii A, Sun Z, Slesarev A, Alemany L B, Lu W and Tour J M 2010 *ACS Nano* **4** 4806
[35] Thomas B J C, Boccaccini A R and Shaffer M S P 2005 *J. Am. Ceram. Soc.* **88** 980–2
[36] Gutierrez D H, Peaslee D, Tanaka Z, Londono N, Meyyapan M and Chen B 2013 *ECS Trans.* **45** 1–11
[37] Cui X, Lee G H, Kim Y D, Arefe G, Huang P Y, Lee C H and Hone J 2015 *Nat. Nanotechnology* **10** 534–40
[38] Dong X, Xing G, Chan-Park M B, Shi W, Xiao N, Wang J, Yan Q, Sum T C, Huang W and Chen P 2011 *Carbon* **49** 5071–8
[39] Díez-Betriu X, Álvarez-García S, Botas C, Álvarez P, Sánchez-Marcos J, Prieto C, Mendez R and de Andrés A 2013 *J. Mater. Chem.* C **1** 6905–12